Available online at www.sciencedirect.com
SCIENCE DIRECT
Optics Communications 261 (2006) 376–380
OPTICS COMMUNICATIONS
www.elsevier.com/locate/optcom

In vivo non-mechanical scanning grating-generated optical coherence tomography using an InGaAs digital camera

Yuuki Watanabe *, Kazuhiko Yamada, Manabu Sato

Graduate School of Science and Engineering, Yamagata University, 4-3-16 Johnan, Yonezawa, Yamagata 992-8510, Japan

Received 28 September 2005; received in revised form 12 December 2005; accepted 13 December 2005

Abstract

We demonstrated in vivo cross-sectional imaging of human fingers by non-mechanical scanning optical coherence tomography (OCT), using a diffracted light as the reference beam and a linear illumination beam at a center wavelength of 1.3 μm for deeper penetration into biological tissues. By applying the three-step phase-shifting method, our system can measure OCT images at 10 frames/s with a sensitivity of 90 dB for a 2.45×4.80 mm (axial × lateral) measurement range using an InGaAs digital camera (320×256 pixels).

1. Introduction

Optical coherence tomography (OCT) is a promising biomedical application that permits cross-sectional imaging of biological tissues with high spatial resolution (~10 μm) to depths of a few millimeters [1]. Time domain (TD) OCT has been used to obtain cross-sectional images of living biological tissues using a grating-based rapid scanning optical delay line with a repetition rate of up to a few kilohertz [2]. However, rapid image acquisition is limited by the necessity for mechanical scanning in two directions (axial and lateral). Spectral domain (SD) OCT techniques have been shown to provide 50 times faster OCT imaging using a one-dimensional line camera and one mechanical lateral scan [3–5].

Two-dimensional (2D) detection devices such as a CCD camera have been used to demonstrate full-field OCT methods that can measure *en-face* images without bidirectional transverse mechanical scanning [6–14]. Sinusoidal phase modulations have been applied to full-field OCT imaging using a photoelastic modulator [6,7] and a PZT [8]. Since these methods measure four interference images at 200 frames/s, an OCT image can be obtained at 50 frames/s. An image acquisition rate of 100 frames/s has been achieved with a pair of CCD cameras [9]. The single-shot imaging technique, which acquires four interferograms simultaneously using only a CCD camera, can capture rapidly moving samples [10,11]. The temporal resolution of this imaging technique depends on the frame rate of the CCD camera. However, the optical setup requires the introduction of four phase-stepped images and is complex. The image size of the resulting tomogram is one-quarter of the captured image size. The full-field OCT can provide longitudinal cross-sectional OCT images from three-dimensional volume data acquired by single axial scanning. Therefore, a high-speed camera is needed to image biological tissues in vivo.

Alternative *en-face* imaging has been demonstrated using a parallel detection scheme using two-dimensional smart pixel silicon detector arrays [12–14]. Each pixel in the detector array has associated electronics to extract the heterodyne signal generated by the scanning reference mirror. Currently, an array of 58×58 pixels has been achieved and this technique has also been used to demonstrate three-dimensional OCT imaging at video rate [14].

Two-dimensional detection SD–OCT has been demonstrated to obtain longitudinal cross-sectional images without axial and lateral scanning [15]. More recently, this technique has been developed with a line illumination

* Corresponding author. Tel./fax: +81 238263292.
E-mail address: ywata@yz.yamagata-u.ac.jp (Y. Watanabe).

0030-4018/$ - see front matter © 2005 Elsevier B.V. All rights reserved.
doi:10.1016/j.optcom.2005.12.030

and a two-dimensional CCD camera for three-dimensional shape measurement [16] and in vivo real-time imaging of human eye structures [17]. In this case, the number of pixels in the axial direction is one-half of the captured size. To obtain OCT images, each A-line has to be mapped and interpolated from wavelength- to k-space and subsequently Fourier transformed [18].

In general, the scattering of light inside the biological tissue is the dominant factor limiting the imaging penetration depth. Since the scattering becomes weaker at longer wavelengths, the use of a light source with longer wavelengths can markedly improve the penetration depth [19,20]. Since indium gallium arsenide (InGaAs) detectors are highly sensitive at near-infrared wavelengths from 900 to 1700 nm, well beyond the range of silicon detectors, the OCT system based on an InGaAs camera is effective for imaging the deeper regions of biological tissues [21]. However, the frame rate and the number of pixels of the InGaAs cameras (typically 30 frames/s for 320×256 pixels) are lower than those of silicon CCD cameras and they are therefore unsuitable for application in the above-mentioned OCT techniques.

In this paper, we describe the application of grating-generated coherence microscopy [22] to an InGaAs digital camera system for in vivo OCT imaging. By use of this method, we can measure the axial interference image of a sample without axial and lateral mechanical scans. In Ref. [22], imaged glass plates were used to demonstrate the principle and it has not been previously possible to demonstrate the experimental sensitivity and imaging of a biological sample. The OCT images were calculated using five interference images that were recorded with a random phase shift. The residual fringes still present in the calculated images result in a decreased sensitivity. We applied a three-step phase-shifting method to improve the experimental sensitivity with the minimum number of frames. In vivo OCT images can be displayed at 10 frames/s with a sensitivity of 90 dB.

2. Experimental setup

A schematic of our imaging system is shown in Fig. 1. The collimated output of a superluminescent diode (Qphotonics, L.L.C, SLD QSDM-1300-9, center wavelength: $\lambda_0 = 1310$ nm, -3 dB spectral width: $\Delta\lambda = 30$ nm) was divided at a non-polarizing beam splitter into signal and reference beams. The diffraction grating was installed in the Littrow configuration such that the mth order diffracted light propagates backward along the incoming path at the reference beam. The Littrow angle θ is determined by

$$2\sin\theta = m\lambda/p, \quad m = 0, 1, 2\ldots, \tag{1}$$

where λ/p is the wavelength-to-period ratio. We used a blazed diffraction grating of 12.7×12.7 mm size, 1.67 μm period, $\theta = 23.14°$ first-order Littrow angle, and 85% diffraction efficiency for 1310 nm. The path difference generated by the diffraction grating is given by

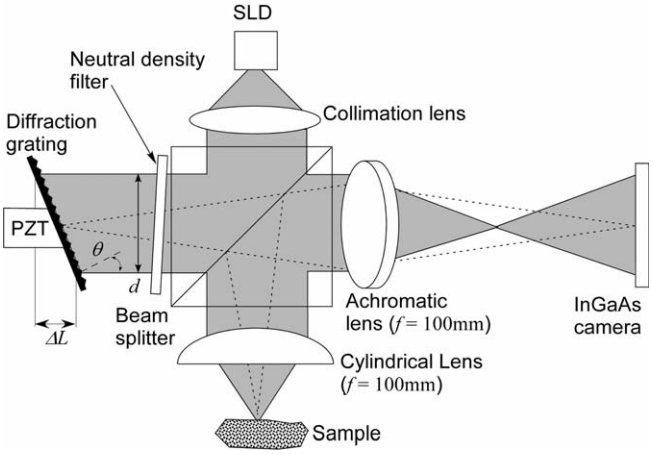

Fig. 1. Schematic of grating generated optical coherence tomography. Dash line is imaging ray.

$$\Delta L = d\tan\theta, \tag{2}$$

where d is the beam diameter. A cylindrical lens ($f = 100$ mm) was inserted in the signal arm to illuminate the sample with a linear light beam. The sample and diffraction grating are imaged onto an InGaAs digital camera (Indigo Systems, Alpha-NIR, 320×256 pixels, 12-bit resolution, 30 frames/s) by an achromatic lens ($f = 100$ mm). The observed interference image $I(x, z)$ is described as:

$$I(x,z) = I_s + I_r + 2(I_r I_i[R_s(x,z) \otimes |\gamma(z)|])^{1/2}\cos(\phi_s - \phi_r), \tag{3}$$

where I_s, I_r, and I_i are the intensities of the sample beam, reference beam, and incident beam, respectively; R_s is the distribution of the sample reflectance; $\gamma(z)$ is the amplitude of the modulation, which is determined by the degree of coherence of the light source; ϕ_s and ϕ_r are the respective phases of the sample and reference beams; and denotes the sign of convolution operator lacks. The diffraction grating was placed on a PZT to shift the phase difference between the signal and reference beams. We acquired three interference images at one-third wavelength intervals corresponding to reference phase differences of 0, $2/3\pi$, and $4/3\pi$ and then calculated an image as follows:

$$\begin{aligned} S &= \left[(2I_{2/3\pi} - I_0 - I_{4/3\pi})^2 + 3(I_0 - I_{4/3\pi})^2\right]\Big/9 \\ &= 4(I_r I_i[R_s(x,z) \otimes |\gamma(z)|]). \end{aligned} \tag{4}$$

This image relates to the distribution of the sample reflective intensity and corresponds to standard OCT images. The calculated OCT images can be displayed at 10 frames/s using homemade software.

3. Theoretical sensitivity

We estimated the theoretical sensitivity of our imaging system using the noise model in Ref. [7]. Although the number of acquired frames differed from our acquisition, both methods were based on the phase-shifting method.

Therefore, this model can be applied to our system. Shot noise that obeys a Poisson distribution is assumed to dominate over any other noise. The variance of the number of detected photons is equal to the number of detected photons itself. When ξ is the number of photoelectrons stored by each pixel of the camera, the properties of noise v are described as follows:

$$\langle v \rangle = 0 \qquad \langle v^2 \rangle = \xi, \tag{5}$$

where the angle brackets denote a time average. When the interference fringe is zero, the noise of the calculated image can be obtained as:

$$S_{\text{noise}} = \alpha\xi, \tag{6}$$

where α is a numerical factor. The three-step phase-shifting method used is $\alpha = 4/3$. If the camera is operated near its maximum full-well charge storage capacity $\xi_{\max}$, we obtain the following relationship:

$$(1 + C)(R_{\text{r}} + R_{\text{s}} + 2R_{\text{inc}})I_{\text{i}} = \xi_{\max}, \tag{7}$$

where R_{r} and R_{s} are the reflectivities of the reference mirror and sample, respectively; and R_{inc} is the proportion of incoherent light. Here, the fringe contrast C can be expressed as:

$$C = \frac{2\sqrt{R_{\text{r}}R_{\text{s}}}}{R_{\text{r}} + R_{\text{s}} + 2R_{\text{inc}}}. \tag{8}$$

Since noise can be found in the case of zero fringe of interference, the number of photoelectrons in the captured image is expressed as:

$$(R_{\text{r}} + R_{\text{s}} + 2R_{\text{inc}})I_{\text{i}} = \xi. \tag{9}$$

Therefore, the signal S and the noise S_{noise} are rewritten as:

$$S = (2\sqrt{R_{\text{r}}R_{\text{s}}}I_{\text{i}})^2 = \left(\frac{C}{1 + C}\xi_{\max}\right)^2, \tag{10}$$

$$S_{\text{noise}} = \frac{\alpha\xi_{\max}}{1 + C}. \tag{11}$$

The SNR can be obtained as follows:

$$\text{SNR} = \frac{S}{S_{\text{noise}}} = \frac{1}{\alpha}\frac{C^2}{1 + C}\xi_{\max}. \tag{12}$$

Assuming that a SNR of 2 is the limit of sensitivity, the minimum detectable reflectivity $R_{\min}$ is approximated by

$$R_{\min} = \frac{\alpha}{2}\frac{(R_{\text{r}} + 2R_{\text{inc}})^2}{R_{\text{r}}\xi_{\max}}. \tag{13}$$

4. Experimental results

To estimate spatial resolution, we measured a test target (USAF1951), as shown in Fig. 2(a), from which we confirmed that the lateral measurement range was 4.80 mm. Fig. 2(b) shows a microscope image of a test target with an area of 2.8×2.1 mm as a reference. The arrow is the measured line. Fig. 2(c) shows the line profile from point A to point B in Fig. 2(a). We were able to resolve the group

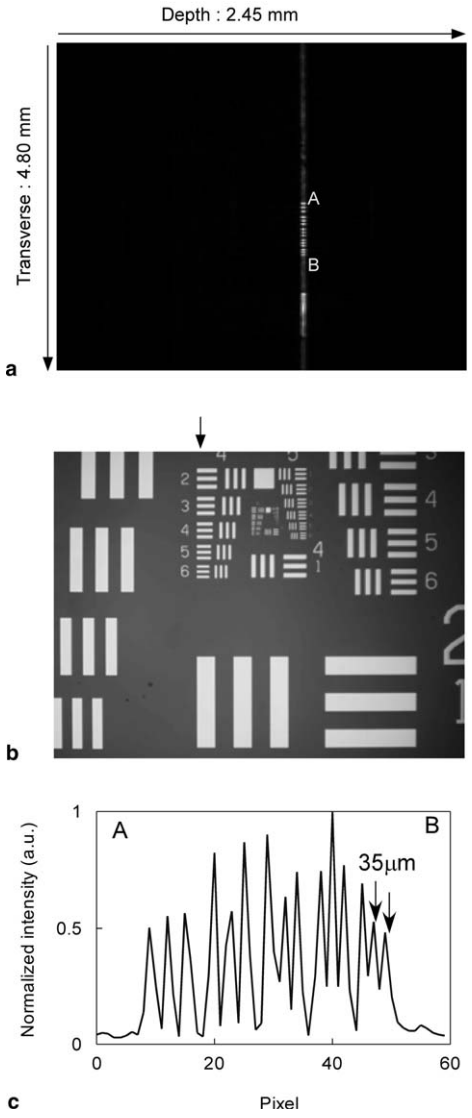

Fig. 2. (a) OCT image of a test target. (b) Microscope image of a test target with the area of 2.8 mm × 2.1 mm. The arrow shows the measured position. (c) Line profile from point A to point B.

4-sixth pattern (28.5 lines/mm) of the test target, which corresponded to a test bar of about 35 μm. Since the focal length of the lens used was long, the influence of the defocus was small. The spatial resolution was degraded by multiple scattering deep in the biological tissues. We measured the peak displacement by moving the test target axially and found that the axial measurement range was $\Delta L =$ 2.45 mm, which corresponded to 7.66 μm/pixel (2.45 mm divided by the 320 pixels of the camera). As expected, a beam diameter of $d = 5.7$ mm was derived from Eq. (2), and the theoretical beam waist of the linear illumination was estimated at $4\lambda f/(\pi d) \sim 29$ μm. However, the experimental value was approximately 58 μm as measured by a beam profiler (Coherent, Beam Master) because of aberrations in the cylindrical lens.

Next, we measured the sensitivity of our OCT system by inserting a plane mirror with an attenuation of −60 dB in

the sample arm, as shown in Fig. 3(a). The reference beam power was adjusted until the pixel values were close to the saturation level of the camera. The experimental sensitivity of our system was approximately 90 dB. We also estimated the theoretical sensitivity of our imaging system using Eq. (13). Our camera had a full-well capacity of $\xi_{max} \approx 18{,}000{,}000$. The reference reflectivity was decided by a neutral-density filter and the diffraction efficiency in the reference arm. We measured a reference reflectivity $R_r = 0.01$ when the measured reflectivity of a plane mirror was $R_r = 1$. Since the sample was a plane mirror, incoherent light was negligible in this measurement. Therefore, these values gave a predicted sensitivity of $10\log(R_{min}) \sim -91$ dB, which was close to the experimental value. The axial profile was rescaled to a linear scale, as shown in Fig. 3(b). The fitted Gaussian curve is also shown in Fig. 3(b). The axial resolution was 26.2 μm in air, which was close to the theoretical value of 24.8 μm.

Finally, we obtained OCT images of a healthy human finger in vivo. Total illumination power used was about 350 μW, which corresponded to an optical power of 1.37 μW per lateral pixel (350 μW divided by the 256 pixels of the camera). When the samples move during acquisition, the contrast in the interference fringe is greatly reduced and the resultant OCT image is degraded. Therefore, the exposure time of the camera was set to 1 ms to avoid blurring and averaging of the interference fringes. These images have been resized to the measurement range and presented on a logarithmic scale. Fig. 4(a) shows the OCT image of a human nail region. The thickness of the nail plate was about 470 μm, assuming the refractive index of a nail to be 1.5. The nail root was visible beneath the skin. Fig. 4(b) shows an OCT image of a human fingertip. We can distinguish between the epidermis and dermis, and sweat gland ducts appear as a spiral structure in the horny layer.

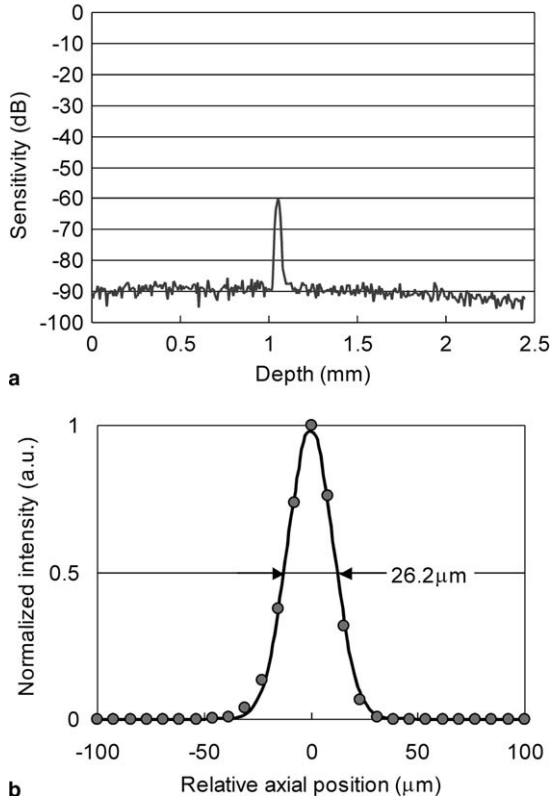

Fig. 3. (a) Sensitivity with an attenuation of −60 dB in the sample arm. (b) Measured axial profile and Gaussian curve fitting.

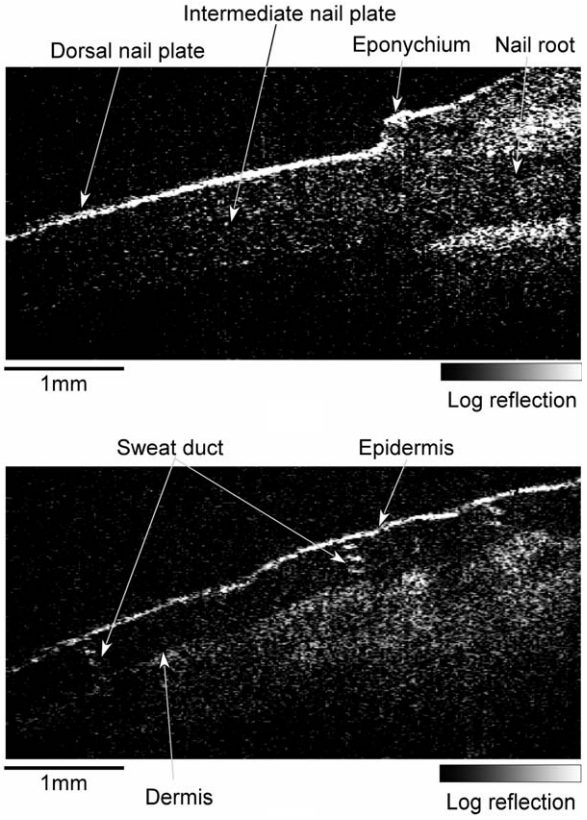

Fig. 4. In vivo OCT images of a healthy human finger. (a) Nail region; (b) fingertip.

5. Discussion and conclusion

We have demonstrated in vivo OCT images using a grating-generated OCT at a 1.3 μm wavelength without a mechanical scan. This system can measure OCT images at 10 frames/s with an imaging area of 2.45×4.80 mm (axial × lateral) using an InGaAs digital camera (320×256 pixels). Since the diffraction grating is only used for the reflected reference beam, a low diffraction efficiency type such as a holographic type grating can be used. In contrast, SD–OCT requires a high efficiency diffraction grating because both signal and reference beams are diffracted by a diffraction grating. Although the frame rate of our system was lower than that of InGaAs SD–OCT [5], the frame rate could be improved to 125 frames/s by using a faster commercially available InGaAs digital camera (Indigo Systems; maximum rate: 345 frames/s).

We have considered improving the axial resolution using a broad spectral light source. In the current system, since one pixel of axial direction corresponds to about 7.7 μm, ultrahigh resolution (1–3 μm) OCT cannot be applied directly. If the measurement size of one pixel corresponds to 1 μm, the maximum measurement range is 320 μm. Therefore, an ultrahigh resolution OCT could be accomplished by narrowing the axial measurement range. Furthermore, our phase-shifting method is by optical path change that depends on wavelength. When the additional phase shift of an interferogram is ϕ_0 at center wavelength λ_0, the resultant phase shift ϕ at another wavelength λ is given by

$$\phi = \phi_0 \lambda / \lambda_0. \tag{14}$$

Since the phase-shift error, which corresponds to the ratio of ϕ to ϕ_0, is about 1% from 1295 to 1325 nm, it would be negligible in the case of the superluminescent diode we used (30 nm-spectral width at center wavelength of 1310 nm). The phase-shift method of ultrahigh resolution OCT is suitable for the achromatic phase shifter based on geometrical phase [23–25].

The 90 dB sensitivity of our system was higher than that of the full-field OCT based on a silicon-CCD camera (82 dB with 1 s acquisition time) [7]. This difference arises because the InGaAs camera has a greater maximum full-well charge storage capacity than a silicon-CCD (typical $\xi_{\max} \approx 2{,}000{,}000$). In general, scattering decreases at longer wavelengths, so OCT image penetration increases. Anderson and Parrish [26] estimated the penetration depth of various wavelengths for which radiation is attenuated to 1/e of the incident radiation density for fair Caucasian skin in vitro. According to Ref. [26], comparing 1.3 μm to 800 nm, the penetration is roughly doubled. Therefore, the InGaAs camera-based OCT can image with more than twice the penetration into biological tissues compared to a silicon-CCD-based OCT at around 800 nm. Compared to Fourier domain OCT, such as InGaAs SD–OCT [5] and swept source OCT [27], although the sensitivity of our system is 15–20 dB lower, it has the advantages of a simple optical configuration and simple signal processing. Therefore, it would be suitable for monitoring OCT images of biological tissues in real time.

In conclusion, we demonstrated a grating-generated OCT with an InGaAs digital camera at 1.3 μm wavelength for deeper penetration into biological tissues. Our system can measure in vivo OCT images (2.45 mm axial × 4.80 mm lateral) at 10 frames/s with a sensitivity of 90 dB. This method does not require a mechanical scan and the OCT image can be obtained by a simple calculation. Therefore, this method would be effective for simple real-time OCT imaging.

Acknowledgment

A part of this study was supported by Industrial Technology Research Grant Program in '05 from New Energy and Industrial Technology Development Organization (NEDO) of Japan.

References

[1] D. Huang, E.A. Swanson, C.P. Lin, J.S. Schuman, W.G. Stinson, W. Chang, M.R. Hee, T. Flotte, K. Gregory, C.A. Puliafito, J.G. Fujimoto, Science 254 (1991) 1178.
[2] A.M. Rollins, M.D. Kulkarni, S. Yazdanfar, R. Ungarunyawee, J.A. Izatt, Opt. Express 3 (1998) 219.
[3] G. Hausler, M.W. Lindner, J. Biomed. Opt. 3 (1998) 21.
[4] M. Wojtkowski, T. Bajraszewski, P. Targowski, A. Kowalczyk, Opt. Lett. 28 (2003) 1745.
[5] S.H. Yun, G.J. Tearney, B.E. Bouma, B.H. Park, J.F. de Boer, Opt. Express 11 (2003) 3598.
[6] M. Lebec, L. Blanchot, H. Saint-jalmes, E. Beaurepaire, A.C. Boccara, Opt. Lett. 23 (1998) 244.
[7] A. Dubois, L. Vabre, A.C. Boccara, E. Beaurepaire, Appl. Opt. 41 (2002) 805.
[8] L. Vabre, A. Dubois, A.C. Boccara, Opt. Lett. 27 (2002) 530.
[9] M. Akiba, K.P. Chan, N. Tanno, Opt. Lett. 28 (2003) 816.
[10] N.B.E. Sawyer, S.P. Morgan, M.G. Somekh, C.W. See, X.F. Cao, B.Y. Shekunov, E. Astrakharchik, Rev. Sci. Instrum. 72 (2001) 3793.
[11] C. Dunsby, Y. Gu, P.M.W. French, Opt. Express 11 (2003) 105.
[12] S. Bourquin, P. Seitz, R.P. Salathé, Opt. Lett. 26 (2001) 512.
[13] M. Ducros, M. Laubsher, B. Karamater, S. Bourquin, T. Lasser, R.P. Salathé, Opt. Commun. 202 (2002) 29.
[14] M. Laubscher, M. Ducros, B. Karamata, T. Lasser, R. Salathé, Opt. Express 10 (2002) 429.
[15] A. Zuluaga, R. Richards-Kortum, Opt. Lett. 24 (1999) 519.
[16] T. Endo, Y. Yasuno, S. Makita, M. Itoh, T. Yatagai, Opt. Express 13 (2005) 695.
[17] B. Grajciar, M. Pircher, A.F. Fercher, R.A. Leitgeb, Opt. Express 13 (2005) 1131.
[18] C. Dorrer, N. Belabas, J. Likforman, M. Joffre, J. Opt. Soc. Am. B 17 (2000) 1795.
[19] J.M. Schmitt, A. Knuttel, M. Yadlowsky, M.A. Eckhaus, Phys. Med. Biol. 39 (1994) 1705.
[20] M.E. Brezinski, G.J. Teaney, B.E. Bouma, J.A. Izatt, M.R. Hee, E.A. Swanson, J.F. Southern, J.G. Fujimoto, Circulation 93 (1996) 1206.
[21] E. Bordenave, E. Abraham, G. Jonusauskas, N. Tsurumachi, J. Oberl, C. Rullière, P. Minot, M. Lassègues, J. Bazeille, Appl. Opt. 41 (2002) 2059.
[22] I. Zeylikovich, A. Gilerson, R.R. Alfano, Opt. Lett. 23 (1998) 1797.
[23] P. Hariharan, M. Roy, J. Mod. Opt. 41 (1994) 2197.
[24] P. Hariharan, M. Roy, Opt. Commun. 126 (1996) 220.
[25] Y. Watanabe, Y. Hayasaka, M. Sato, N. Tanno, Appl. Opt. 44 (2005) 1387.
[26] R.R. Anderson, J.A. Parrish, J. Invest. Dermatol. 77 (1981) 13.
[27] S.H. Yun, G.J. Tearney, J.F. de Boer, N. Iftimia, B.E. Bouma, Opt. Express 11 (2003) 2953.